

# A GENETIC ALGORITHM FOR TRAJECTORY GENERATION IN ENGINE-OUT EMERGENCY LANDING SCENARIOS OF COMMERCIAL AIRCRAFT

Jason Gauci<sup>1</sup>, Brian Zammit<sup>2</sup>, Marlon Galea<sup>3</sup>

<sup>1</sup>Senior lecturer, Institute of Aerospace Technologies, University of Malta <sup>2</sup>Senior lecturer, Department of Electronic Systems Engineering, Faculty of Engineering, University of Malta <sup>3</sup>Research officer, Institute of Aerospace Technologies, University of Malta

#### Abstract

This paper presents a Genetic Algorithm (GA) designed for trajectory generation in engine-out emergency landing scenarios encountered by large transport aircraft. The proposed GA formulates waypoint trajectories considering aircraft performance constraints and energy management, aiming to guide the aircraft to a designated landing site with appropriate speed and height to ensure a safe landing. Simulation results demonstrate the efficacy of the GA in generating feasible trajectories – with different numbers of waypoints – across different emergency scenarios. Future work aims to enhance the GA by incorporating wind effects and developing intuitive cockpit interfaces for pilot interaction. This research contributes to advancing emergency response capabilities in commercial aviation, promoting safety and efficiency in critical flight operations.

Keywords: TLOT, forced landing, trajectory planning, energy management, Genetic Algorithm.

#### 1. Background

Emergency landing occurrences in commercial aviation may be triggered by a range of unforeseen circumstances, such as severe weather conditions, Total Loss of Thrust (TLOT) and other unpredictable events. These situations represent a rare yet very important aspect of safe flight operations which has seen gradual improvement due to the reliability of modern jet engines. However, when pilots face such emergencies, their ability to react effectively becomes critical to ensuring the safety of the aircraft and its passengers.

The flight crew's response to these situations is crucial and involves a series of complex, time-sensitive tasks which significantly increase pilot workload and, consequently, the risk of making incorrect decisions. As a first step, the crew must assess the cause of the emergency and determine the severity of the situation. In some cases, such as with TLOT, an attempt to restart the engines is warranted, especially at high altitudes. If the emergency persists, the crew must select a suitable landing site, ideally an airport – though this may not always be possible – and determine the most efficient route to reach this location. This process involves considering factors such as the proximity of landing sites, current and forecasted weather conditions, and airport facilities. This decision-making process is especially crucial in a TLOT scenario where the aircraft's glide capabilities become a key consideration. Following this selection, the crew need to plan the descent trajectory to accommodate the possibly reduced performance of the aircraft, ensuring that the aircraft reaches the landing site at an appropriate height and speed, and thus with the correct energy level for a safe landing.

Therefore, such situations require the crew to demonstrate exceptional technical skill, situational

awareness, and strategic planning. This highlights the importance of advanced training and preparation but also the necessity of providing on-board decision-making frameworks that support the crew in making timely decisions during these high-workload scenarios, ensuring the safety of everyone on-board. To this effect, in previous work, the authors developed a framework to assist the crew in selecting a suitable landing site by ranking multiple airports and off-airport locations using a fuzzy logic-based system [1]. This work, instead, focuses on supporting the crew in identifying the optimal descent trajectory which allows the aircraft to reach the selected landing site, taking into consideration aircraft performance capabilities and energy management aspects.

#### 2. Literature review

Different trajectory planners are proposed in the literature for emergency landing purposes. A popular approach is based on Dubins path planning. For instance, in [2, 3], Atkins et al present an algorithm which generates a minimum-length best glide Dubins path. This path can be adjusted – either by extending the final approach segment or by inserting an S-turn – to absorb any extra energy. In [4], if a simple Dubins path brings the aircraft to the runway with excess altitude, the algorithm adjusts the path by generating an integral number of spiral turns and/or extending the final approach. A wind-aware version of this algorithm is proposed in [5]. Fallast et al [6] use a route planner based on a modified Rapidly Exploring Random Tree (RRT\*), where the path is defined as a set of Dubins path segments and accounts for aircraft performance and other constraints.

A Dynamic Programming (DP) approach is proposed in [7] and [8]. In [7], a reverse DP approach is adopted whereby the gliding trajectory is computed backwards from the final landing configuration (height, speed and flight path angle) through a set of constraints and space discretised state equations. However, this algorithm does not integrate lateral manoeuvres and ignores the effect of wind. An Approximate DP algorithm – based on Q-Learning – is proposed in [8]; however, this does not account for flight dynamics when generating the emergency trajectories. Meng et al [9] and Miwa et al [10] convert the trajectory planning problem to a Non-Linear Programming (NLP) problem using a direct collocation method. Then, they solve the problem using a Sequential Quadratic Programming (SQP) algorithm. In both cases, the algorithm minimises the duration of the forced landing and takes wind into account.

Avrenli and Dempsey [11] propose a kinematic approach where the trajectory is divided into three types of segments: linear segments, transition segments and circular segments. The proposed algorithm is primarily intended for emergencies at low altitude (below 5,000 feet) and does not cope with situations where the aircraft has more height than needed to fly the trajectory. Therefore, the crew would need to dissipate any excess altitude e.g. by extending the landing gear earlier than usual. A 3D trajectory planner based on motion primitives – including a gliding primitive, velocity adjustment primitive and a constant-rate turning primitive – is proposed in [12]. These primitives can be connected to form basic manoeuvres, and a flight path can be constructed from source to destination by concatenating various manoeuvres. These reduce the planning problem to a graph-search problem of tractable size which is solved using the A\* algorithm.

This work proposes a path planning algorithm which is different from the above and is based on Genetic Algorithms (GAs). As will be shown in the rest of this paper, this algorithm finds a feasible glide path – between the initial aircraft position and the emergency landing site – which accounts for the aircraft's performance and can absorb any excess energy to ensure that the aircraft reaches the landing site in a stabilised configuration and at the right height and speed.

#### 3. Emergency Trajectory Parametrisation

The structure of the emergency flight trajectory was designed to prioritise simplicity, seamless integration into the Flight Management Computer (FMC) for eventual full autopilot control, and ease of execution if the pilot chooses to override the FMC. The trajectory consists of four waypoints, resulting in a lateral path comprising five straight segments and four circular segments as shown in

Figure 1. The number of waypoints in the emergency trajectory is a critical design parameter that needs adequate consideration. To optimise trajectory simplicity while retaining manoeuvrability around high terrain or weather cells, four waypoints were selected. This number strikes a balance between achieving a streamlined trajectory and ensuring enough authority for lateral adjustments. Figure 1 also shows the aircraft's heading changes at each fly-by waypoint ( $\emptyset_i$ , where i = 1..4). The resulting trajectory consists of an initial straight segment - aligned with the aircraft's heading - that provides a buffer zone to reduce cognitive overload, allowing pilots a brief period to assess the situation and transition mentally before the first turn. Waypoint 1 is therefore strategically positioned in line with the aircraft's initial heading, located at a distance  $d_1$  ahead of the aircraft. Similarly, a final leg along the extended runway centreline provides adequate stabilisation distance before touchdown. This alignment minimises the need for corrective manoeuvres during the final approach phase, enhancing safety and reducing the risk of runway excursions. Therefore, Waypoint 4 is aligned with the runway heading, situated at a distance  $d_4$  from the runway threshold. This results in a lateral trajectory consisting of a sequence of straight and curved segments that can be easily uploaded and flown by modern navigation systems capable of executing Required Navigation Performance (RNP) routes.

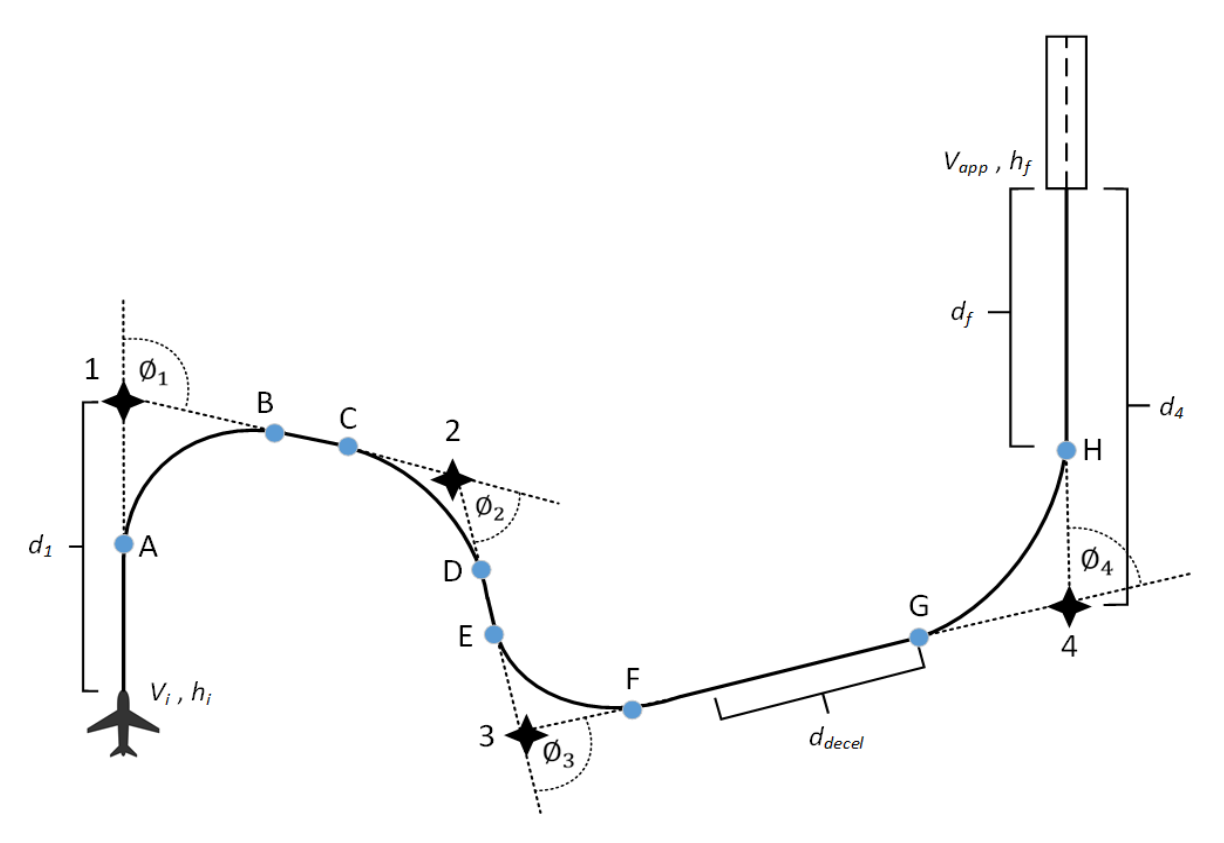


Figure 1 – Lateral profile of emergency flight trajectory.

In the fourth segment, between Waypoints 3 and 4, a deceleration segment, denoted as  $d_{decel}$ , is introduced. This segment facilitates the aircraft's deceleration in level flight from its initial speed,  $V_{i}$ , to the final approach speed,  $V_{app}$ . It is worth noting that  $d_{decel}$  may be shorter than the distance between points F and G. The aircraft crosses the runway threshold at the target energy defined as a function of the approach speed,  $V_{app}$ , and the target height,  $h_f$ , above the runway threshold.

In this work, several critical assumptions have been made to facilitate the design and expedite the execution time during optimisation. Firstly, it is assumed that the initial height,  $h_i$ , of the aircraft does

not exceed Flight Level (FL) 200. This ensures that the aircraft is always below the crossover altitude, which results in a constant green dot speed  $V_{gdot}^{1}$ . The aircraft speed at the start of the trajectory is assumed to coincide with  $V_{gdot}$ . This eliminates the need to introduce deceleration segments at the start of the path, which would increase the computation time of the trajectory. The green dot speed was set to 225 knots<sup>2</sup> based on an Airbus A320 weighing 70 tons and operating at or below FL 200 [13]. At this speed, a glide ratio ( $GR_0$ ) of around 15.2 is expected, translating to a glide distance of 2.5 nautical miles (NM) per 1000 feet (with no wind).

The approach speed,  $V_{app}$ , is established at 166 knots, reflecting typical landing conditions with landing gear deployed and flaps set to configuration 2 (CONF 2). At this speed, a glide ratio ( $GR_0$ ) of around 9.72 is expected, translating to a glide distance of 1.6 nautical miles (NM) per 1000 feet (with no wind). Moreover, the aircraft's deceleration from  $V_{gdot}$  to  $V_{app}$  is assumed to occur at a rate of approximately 20 knots per nautical mile. The true airspeed is assumed to be equal to  $V_{gdot}$  up to the beginning of the level deceleration segment (defined by  $d_{decel}$ ), and equal to  $V_{app}$  from the end of the level deceleration segment up to the landing. Additionally, it is assumed that the aircraft can execute instantaneous banking manoeuvres, simplifying the geometry of the trajectory calculations. Finally, wind is assumed negligible, which also simplifies the analysis by supressing any lateral shifts that would occur in windy conditions.

To determine the radius of the turn at each fly-by waypoint, a simplified point-mass model of an aircraft was used. A constant average ground speed was computed at the middle of the turn and assumed to be valid throughout the entire turn segment. Given the average ground speed,  $V_g$ , and the bank angle,  $\theta$ , the turn radius can be found using Eq. 1, where g is the acceleration due to gravity.

$$R = \frac{V_g^2}{g \tan \theta} \tag{1}$$

The glide ratio,  $GR_{\theta}$ , of the aircraft at any point along the trajectory is a function of the glide ratio at wings level,  $GR_{0}$ , and decreases proportionally with the bank angle  $\theta$ , as shown in Eq. 2 below.

$$GR_{\theta} = GR_0 cos\theta \tag{2}$$

# 4. The Genetic Algorithm

#### 4.1 Genes and chromosomes

For the GA, each candidate solution within the population comprises of a set of properties referred to as chromosomes, which define a lateral trajectory based on the parametrisation outlined in Figure 1. Each chromosome consists of 10 genes as detailed in Table 1, where  $d_1$  signifies the distance between the initial position of the aircraft and Waypoint 1, and  $d_4$  represents the distance between Waypoint 4 and the final position of the aircraft (i.e. the runway threshold). The coordinates of the intermediate waypoints are determined by Genes 2 to 5, where  $x_1$  and  $y_2$  denote the coordinates of Waypoint 2 and  $x_2$  and  $y_2$  represent the coordinates of Waypoint 3.<sup>3</sup> Genes 7 to 10 specify the required bank angle ( $\theta_i$ , where i = 1..4) at each waypoint along the trajectory.

<sup>&</sup>lt;sup>1</sup> This is the best lift-to-drag ratio speed.

<sup>&</sup>lt;sup>2</sup> Below FL200, a rough estimate for the green dot speed in clean configuration is 2 x weight (tons) + 85 kts.

<sup>&</sup>lt;sup>3</sup> The x and y coordinates correspond to the lateral position of the aircraft. The vertical position of the aircraft is calculated based on its glide performance.

Table 1 – Definition of the genes in the chromosome.

G1	G2	G3	G4	G5	G6	G7	G8	G9	G10
$d_1$	<b>X</b> 1	<b>y</b> 1	<b>X</b> 2	<b>y</b> 2	d₄	$ heta_1$	$ heta_2$	$\theta_3$	$ heta_4$

To constrain the problem's search space, bounds are defined for each gene in the chromosome. The lower and upper bounds of the first six genes are adjusted based on the maximum glide distance of the aircraft to ensure that the candidate trajectories do not extend beyond this distance. Meanwhile, bounds for the last four genes – specifying the aircraft's bank angles – are set to +/- 30°.

The performance of the GA can be influenced by the setup of the initial population, and therefore valid candidate solutions should be used. To this effect, the candidate trajectories' initial population is set up using the shortest straight-line trajectory from the initial position of the aircraft to the runway threshold. The first six genes of each chromosome are randomly initialised along the shortest path, while genes corresponding to the bank angles are set to values between their lower and upper bounds.

The resulting optimisation problem was formulated in MATLAB and solved using the GA function "ga", where several parameters were configured to guide the optimization process [14]. The population size was set to the default value of 200 individuals, striking a balance between execution speed and performance. The elite count, also set to the default value of 10, specifies the number of top-performing individuals that are preserved from one generation to the next without undergoing crossover or mutation, thus maintaining diversity within the population and preventing premature convergence to suboptimal solutions. The crossover fraction was configured to 0.4 and represents the proportion of the population subject to crossover during each generation. The default MATLAB crossover scattered function was retained for crossover, selecting random subsets of genes from two parent individuals and exchanging them to create offspring individuals. Similarly, the selection and mutation functions were left unchanged and set to the default MATLAB functions that implement selection mechanisms and mutation operations to introduce genetic diversity into the population.

#### 4.2 Fitness Function and Constraints

To define the fitness function of the GA, it was necessary to establish criteria for an optimal emergency trajectory. This led to the following target optimisation objectives:

- Minimise heading changes This objective aims to reduce unnecessary heading changes, simplifying the geometry of the lateral trajectory. The minimum threshold for the total heading change is scenario-dependent and defined as the difference between the initial aircraft heading and the runway heading.
- 2. **Maximise final distance** Maximising the distance between the end of the final turn and the runway threshold, *d<sub>i</sub>*, enhances the stabilisation distance before landing. Increasing this distance also promotes earlier heading changes along the trajectory, reducing the risk of late-stage manoeuvres close to the ground. However, to balance this objective with the need for manoeuvring space in the initial part of the trajectory, a target value of approximately 1 NM was found to be adequate.
- 3. **Minimise bank angles** This objective aims to minimise the sum of bank angles along the trajectory, promoting shallower turns as the aircraft loses height. This reduces the likelihood of a stall close to the ground.

To incorporate these objectives, a fitness function involving a weighted sum of costs was implemented as follows:

$$C = ||C_1|| + ||C_2|| + ||C_3|| \tag{3}$$

where  $C_1$  represents the total heading change along the trajectory, computed by summing the heading changes at each waypoint (Eq. 4).  $C_2$  defines the cost for the extent of final distance allowance  $d_i$ , with an exponential function heavily penalising distance values smaller than 1 NM (Eq. 5). Finally,  $C_3$  defines the cost for the bank angles selected at each waypoint, with a banking weight defined at each waypoint to promote smaller banking values closer to the runway (Eq. 6). A total weight value of unity was set by defining  $W_i$  as follows:  $W_1 = 0.05$ ,  $W_2 = 0.05$ ,  $W_3 = 0.2$  and  $W_4 = 0.7$ .

$$C_1 = \sum_{i=1}^4 \phi_i \tag{4}$$

$$C_2 = e^{-(d_f - 1)} - 1 (5)$$

$$C_3 = \sum_{i=1}^4 W_i \theta_i \tag{6}$$

The optimisation problem was constrained using one equality and two inequality constraints as shown in Eqs. 7-9.

$$h_f = 50 feet (7)$$

$$d_{FG} \ge 2.95 \text{NM} \tag{8}$$

$$d_{a_i} + d_{b_i} \le d_i \tag{9}$$

The first constraint (Eq. 7) captures the energy requirement as the aircraft crosses the runway threshold at the approach speed. The second constraint (Eq. 8) relates to the distance required for the aircraft to decelerate from green dot speed to approach speed, requiring a minimum distance  $d_{FG}$  of 2.95 NM. Finally, the third constraint (Eq. 9) ensures continuity of the lateral path for consecutive fly-by waypoints. As depicted in Figure 2, should the selected distance  $d_i$  be too small, the aircraft cannot fly along the candidate path. In such a case, the end of the first turn segment 'a' would overfly the start of the second turn segment 'b'. The trajectory is continuous when the total distance  $d_{a_i}$  and  $d_{b_i}$  is shorter than the waypoint separation distance  $d_i$ .

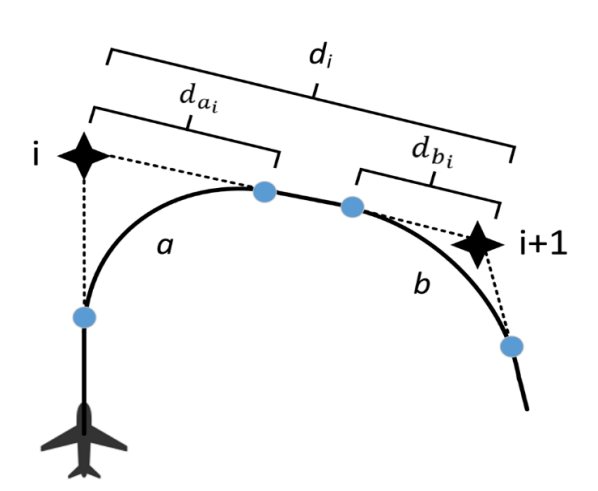


Figure 2 – Defining the continuity constraint for fly-by waypoints.

# 5. Simulation testing and results

Section 3 described an emergency flight trajectory consisting of four waypoints. However, this definition – and the corresponding GA – can be easily extended to cater for a different number of waypoints. Consequently, this section presents results obtained with three different configurations of the GA – corresponding to three, four or five waypoints.

The GA was tested by simulating various forced landing scenarios and changing the following parameters in each scenario: initial aircraft heading ( $HDG_A$ ), initial aircraft height ( $h_i$ ), runway position ( $x_R$ ,  $y_R$ )<sup>5</sup> and runway heading ( $HDG_R$ ). The initial lateral aircraft position ( $x_A$ ,  $y_A$ ) was kept the same in all the test scenarios ( $x_A$ =100 NM,  $y_A$ =100 NM). The tests were carried out on an Apple M1 Pro processor with 16 GB of RAM using MATLAB R2021b. In each test, the GA was allowed to run for 50 generations. Table 2 lists the simulated scenarios.

Table 2 – Test scenarios.

#	HDG <sub>A</sub> (°)	h <sub>i</sub> (feet)	$x_R(NM), y_R(NM)$	HDG <sub>R</sub> (°)
1	90	5,000	(110, 102)	90
2	0	5,000	(102, 110)	0
3	315	5,000	(95, 101)	90
4	300	5,000	(97, 95)	90
5	90	5,000	(103, 94)	0
6	45	10,000	(110, 113)	0
7	0	10,000	(101, 120)	0
8	0	10,000	(90, 110)	90
9	280	10,000	(95, 105)	270
10	90	10,000	(101, 85)	360
11	225	10,000	(95, 85)	360
12	0	10,000	(99, 80)	360
13	270	10,000	(100, 100)	90
14	15	15,000	(105, 130)	180
15	145	15,000	(110, 70)	10
16	180	15,000	(80, 115)	45
17	315	15,000	(75, 110)	0

#### 5.1 Results with four waypoints

The first set of results – corresponding to a subset of the test scenarios – is shown in Table 3 and Figs 3-8. Table 3 shows the results corresponding to the GA's fitness function, whereas Figs. 3-8 show the lateral and vertical profiles of the emergency trajectory in different scenarios. The vertical profile of the emergency trajectories shows how the glide ratio of the aircraft changes along the

<sup>&</sup>lt;sup>5</sup> Runway position corresponds to the runway threshold.

trajectory, and also shows the level flight deceleration before the final turn.

As can be observed, the GA manages to find a feasible solution in each case while satisfying all of the constraints. In certain cases, the length of a straight or circular segment is very short; for instance, in Scenario 10, points D and E practically overlap each other (Figure 5). This leads the aircraft to only perform three turn maneuvers (instead of four, as expected). From Table 3 it can be seen that the final bank angle ( $\theta_4$ ) is not always the smallest of the bank angles, even though it is penalized the most. Also, the length of the final approach segment (given by  $d_f$ ) varies from one scenario to another but is never less than 1 NM – in line with one of the objectives of the fitness function.

Despite running the GA for 50 generations, it was observed that convergence typically occurred within the first few generations. This phenomenon underscores the effectiveness of the GA in quickly exploring and exploiting the solution space to identify optimal or near-optimal solutions. Such rapid convergence suggests that the initial population was sufficiently diverse, allowing the algorithm to efficiently navigate towards promising regions of the search space.

Similar results and patterns were observed in the rest of the test scenarios provided in Table 2.

Scenario	$\theta_i$ (°)	Δ <i>HDG</i> (°)	d <sub>f</sub> (NM)	Execution time (s)
4	$\theta_1$ = 29.59, $\theta_2$ = 22.27, $\theta_3$ = 21.82, $\theta_4$ = 28.67	233.71	2.47	216.41
10	$\theta_1$ = 24.80, $\theta_2$ = 29.88, $\theta_3$ = 28.50, $\theta_4$ = 29.75	450.00	1.04	200.18
16	$\theta_1$ = 27.31, $\theta_2$ = 29.82, $\theta_3$ = 27.83, $\theta_4$ = 14.44	308.97	4.05	203.53

Table 3 – Results associated with the fitness function.

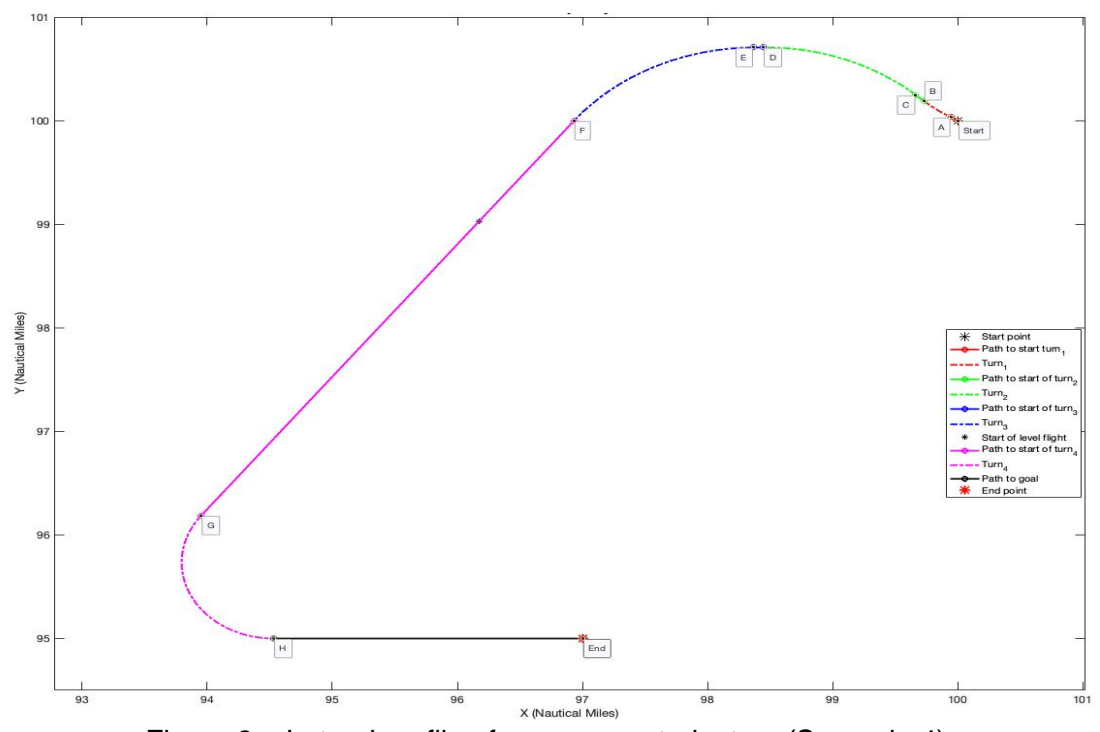


Figure 3 – Lateral profile of emergency trajectory (Scenario 4).

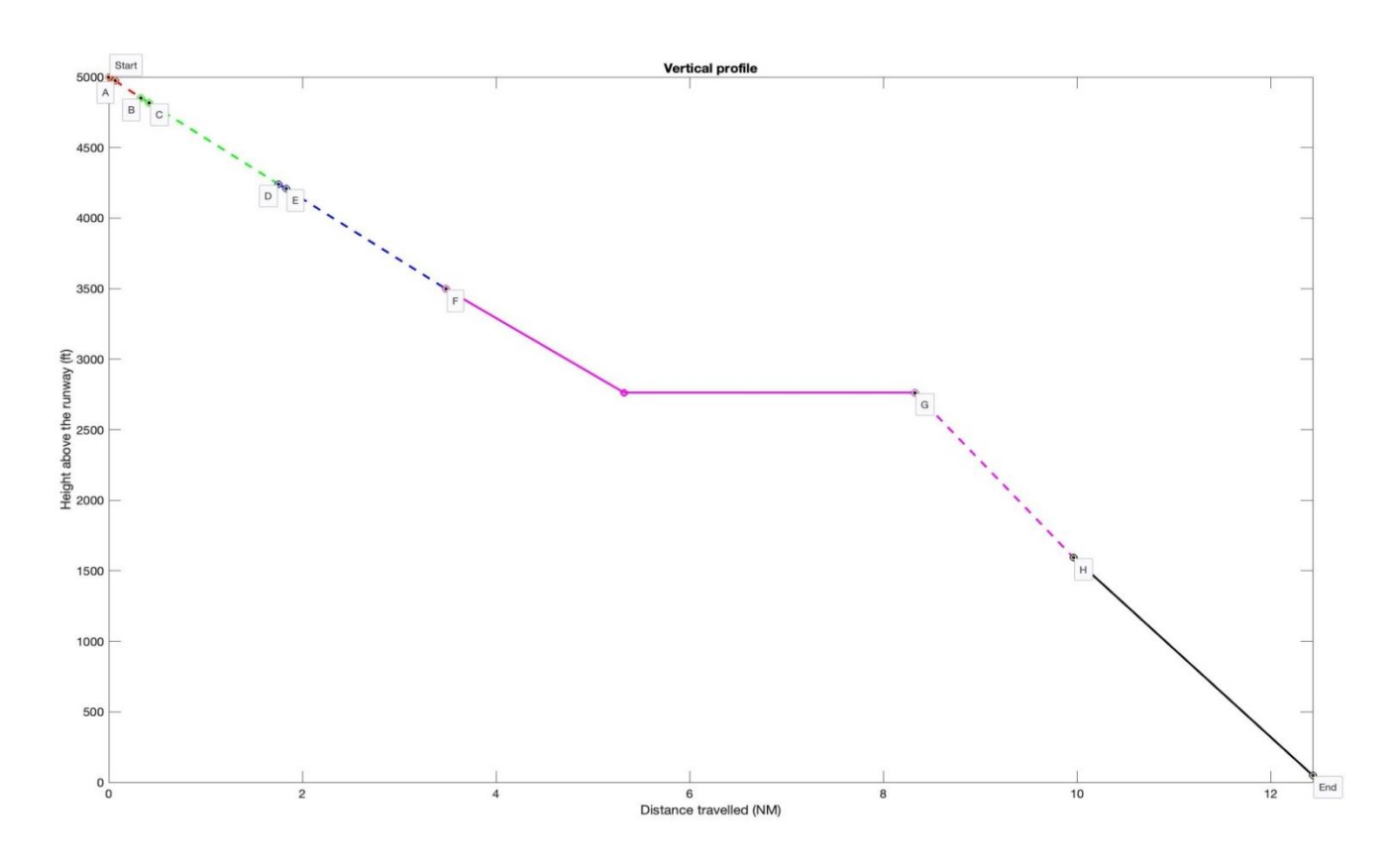


Figure 4 – Vertical profile of emergency trajectory (Scenario 4).

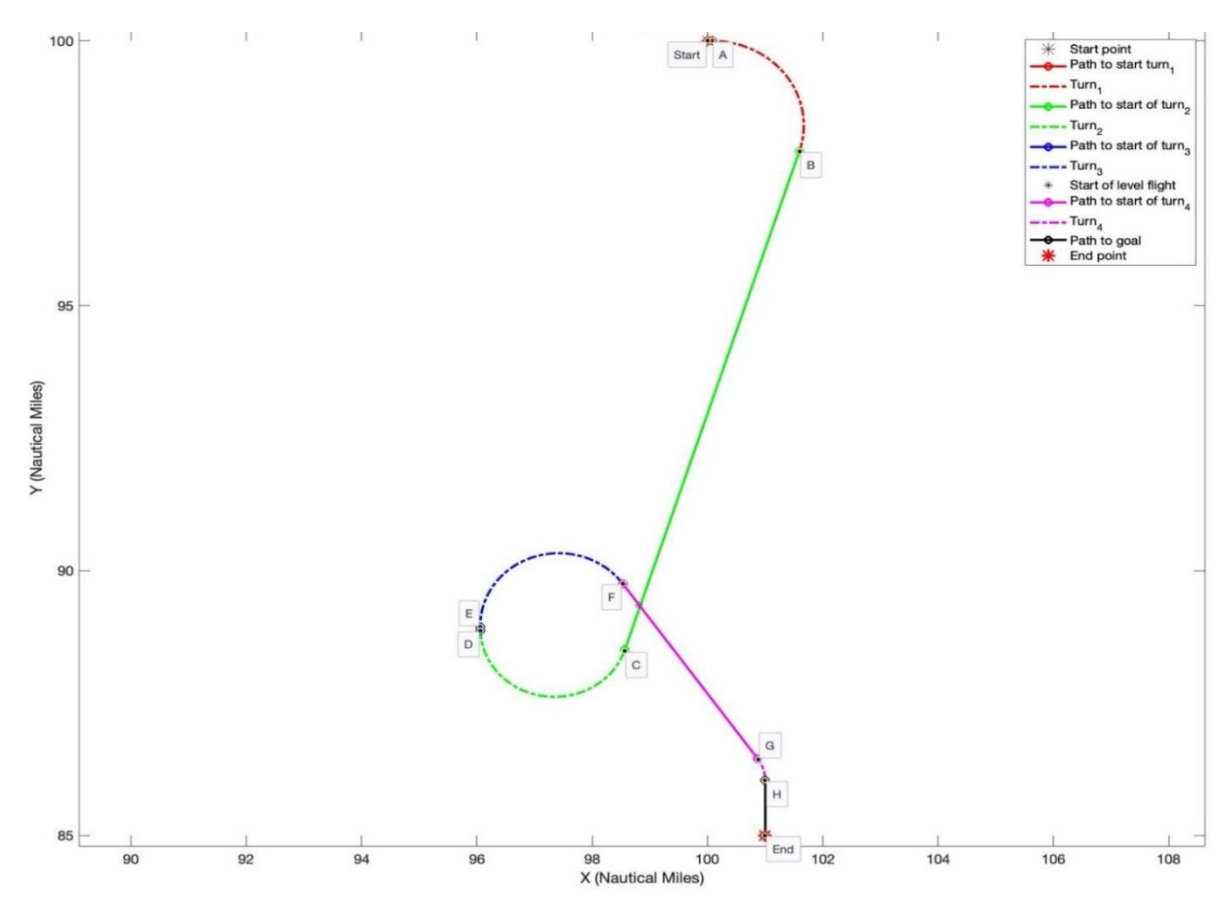


Figure 5 – Lateral profile of emergency trajectory (Scenario 10).

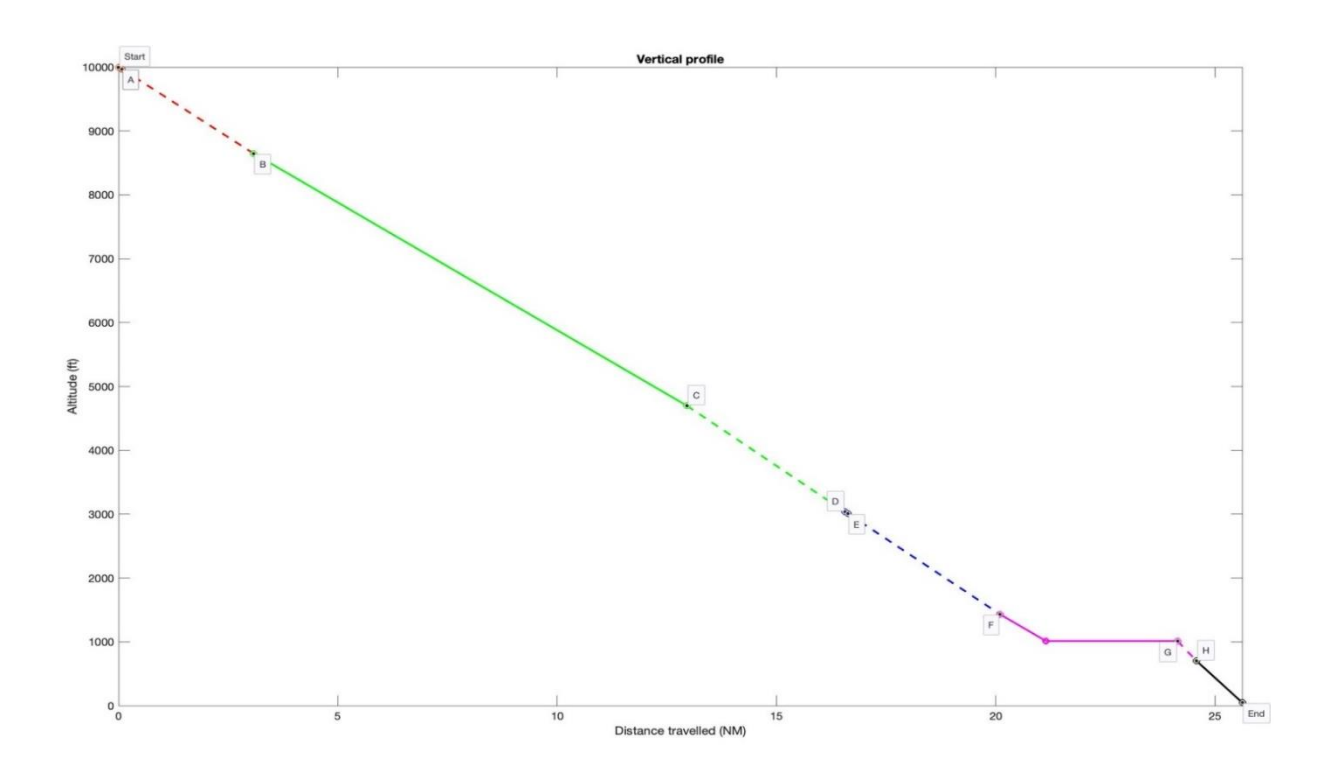


Figure 6 – Vertical profile of emergency trajectory (Scenario 10).

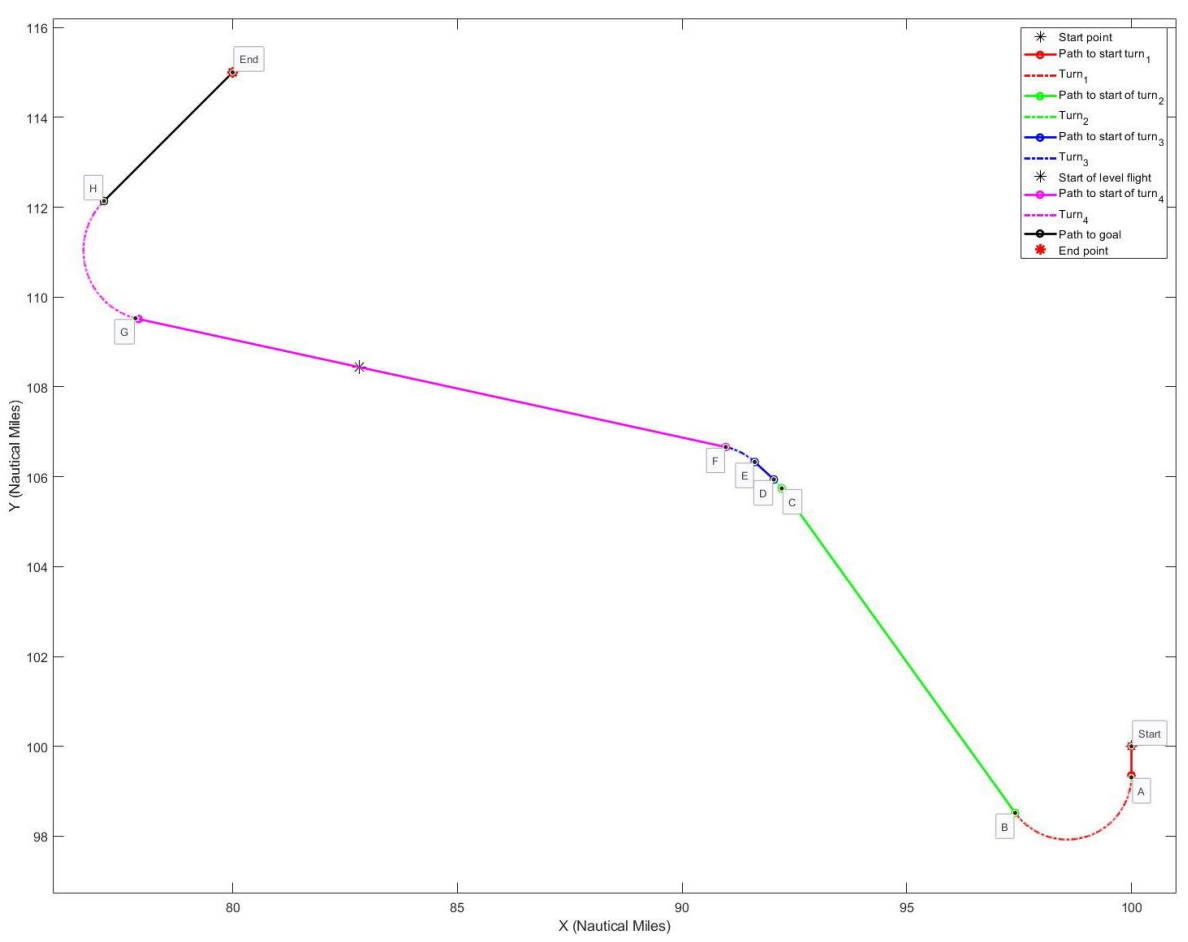


Figure 7 – Lateral profile of emergency trajectory (Scenario 16).

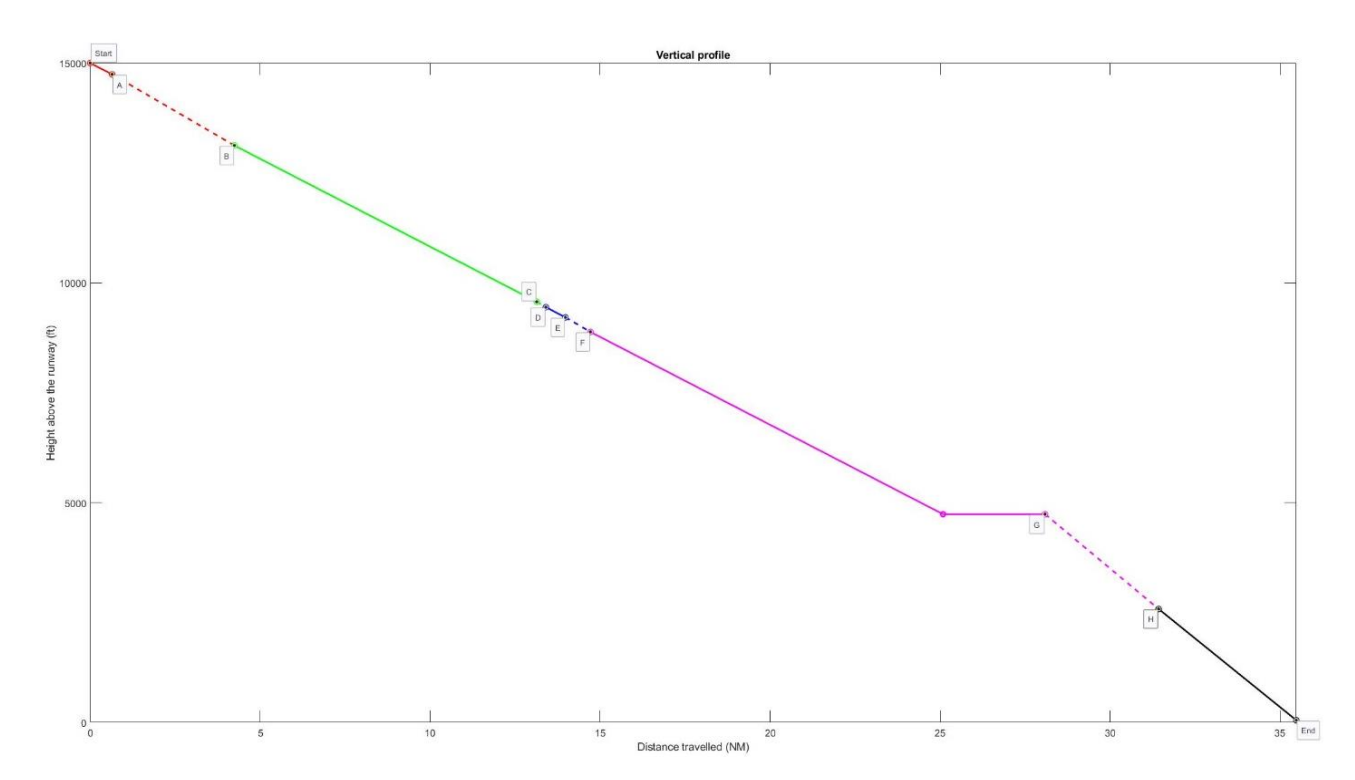


Figure 8 – Vertical profile of emergency trajectory (Scenario 16).

Figures 9 and 10 show the results obtained for the special case when the aircraft is directly above the runway (Scenario 13). Some of the algorithms proposed in the literature either struggle or fail to provide a solution in this case (e.g. [2, 4]). On the other hand, the proposed GA manages to find a solution even in this case by proposing a teardrop trajectory.

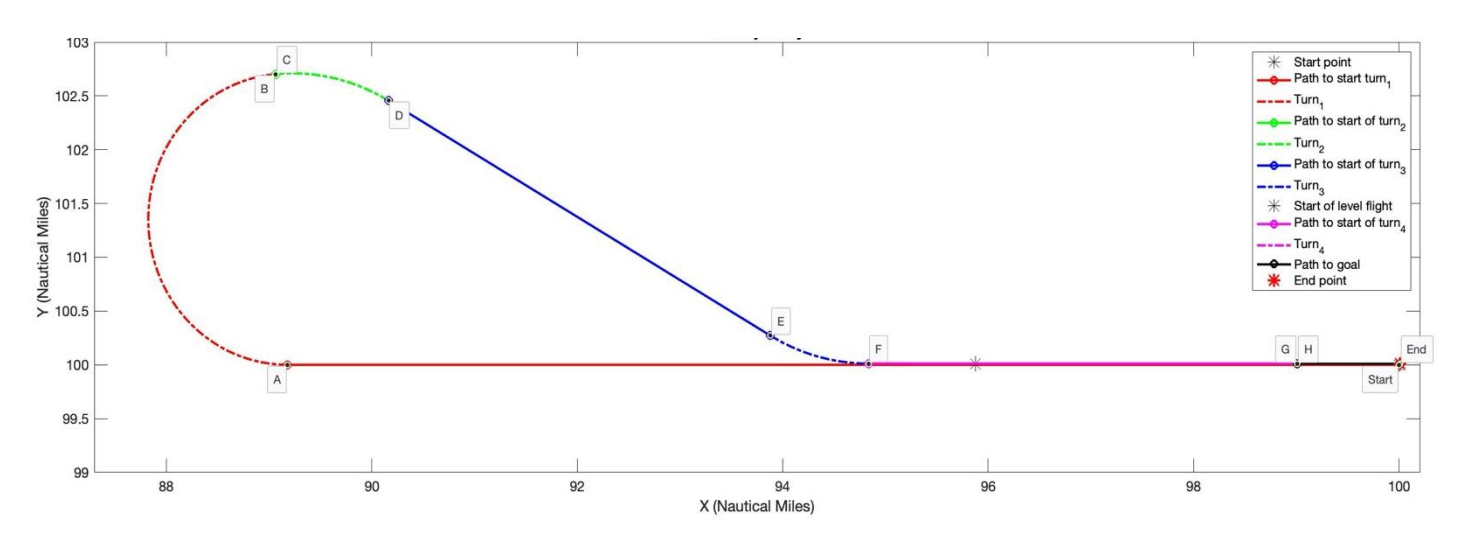


Figure 9 – Lateral profile of emergency trajectory (Scenario 13).

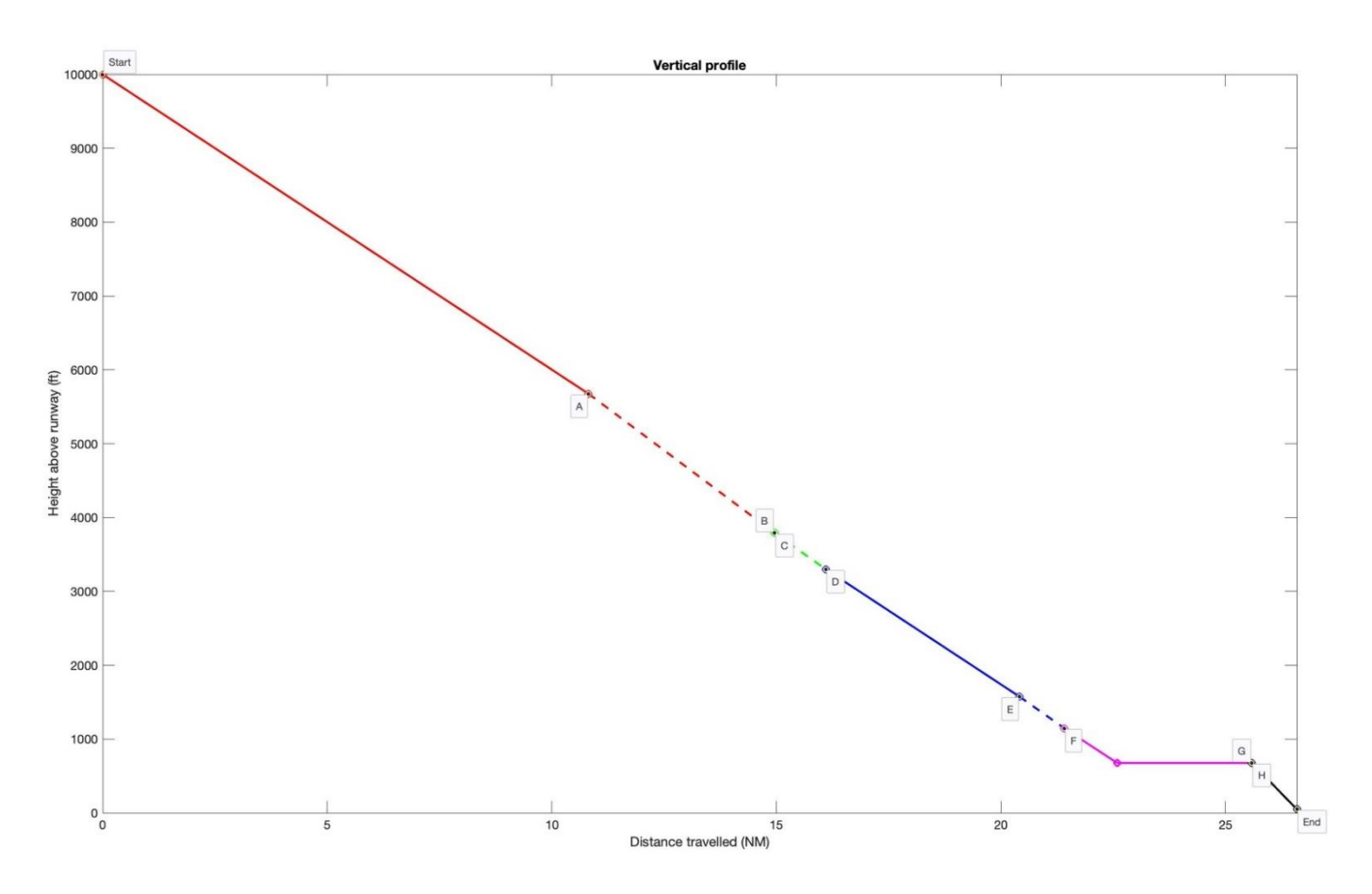


Figure 10 – Vertical profile of emergency trajectory (Scenario 13).

## 5.2 Results with three, four and five waypoints

Table 4 and Figure 11 show the results obtained when the GA is configured to generate trajectories with three waypoints in Scenario 2. In this case, the scenario is repeated for different values of  $h_i$ . It can be observed that, as the initial aircraft height increases, the lateral path of the emergency trajectory is elongated sideways to absorb the extra potential energy of the aircraft. Consequently,  $\Delta HDG$  also increases with height. This is expected given the fixed number of waypoints of the trajectory. On the other hand,  $d_f$  decreases with height but never falls below 1 NM, in line with one of the objectives of the fitness function. Also, in all of the scenarios – except at 5,000 feet – the final bank angle is the smallest, in line with another objective of the fitness function.

Table 5 and Figs. 12-13 show the results obtained when the GA is configured to generate trajectories with five waypoints in Scenario 9. It can be observed that points F and G are practically on top of each other, meaning that the aircraft performs a single, continuous turn manoeuver between points E and H. Having a larger number of waypoints is particularly beneficial when it is necessary to navigate around obstacles (e.g. adverse weather or high terrain) that may be present between the aircraft and the runway. It also allows the aircraft to lose more energy in turn segments.

Finally, Tables 6-8 and Figs. 14-16 show the results obtained in Scenarios 5, 6 and 17 when the GA is configured to generate trajectories with three, four and five waypoints. It can be observed that, in the case of Scenario 6, the three trajectories are similar in overall shape and approximate an S-turn; however, this is not the case for the other two scenarios. As expected,  $\Delta HDG$  tends to increase with number of waypoints as the aircraft executes more turns; however, in the case of the five-waypoint trajectories, one of the heading changes is 0 (or almost equal to 0), leading the aircraft to perform

one less turn than expected. This is desirable as it simplifies the emergency trajectory. Distance  $d_t$  is at least 1 NM in all cases.

Table 4 – Results associated with the fitness function (Scenario 2).

h <sub>i</sub> (feet)	$\theta_i$ (°)	Δ <i>HDG</i> (°)	d <sub>f</sub> (NM)	Execution time (s)
5,000	$\theta_1$ = 25.66, $\theta_2$ = 29.86, $\theta_3$ = 28.86	210.44	2.40	193.97
7,000	$\theta_1$ = 29.40, $\theta_2$ = 28.58, $\theta_3$ = 12.72	282.45	1.54	190.48
9,000	$\theta_1$ = 29.90, $\theta_2$ = 29.69, $\theta_3$ = 13.72	303.21	1.08	191.13
10,000	$\theta_1$ = 29.36, $\theta_2$ = 29.50, $\theta_3$ = 14.72	313.73	1.09	188.59
13,000	$\theta_1$ = 28.01, $\theta_2$ = 29.85, $\theta_3$ = 13.07	330.92	1.12	196.25
15,000	$\theta_1$ = 29.39, $\theta_2$ = 29.84, $\theta_3$ = 17.51	330.30	1.06	194.31

Table 5 – Results associated with the fitness function (Scenario 9).

$\theta_i$ (°)	∆ <i>HDG</i> (°)	df (NM)	Execution time (s)
$\theta_1$ = 16.30, $\theta_2$ = 18.68, $\theta_3$ = 30.00, $\theta_4$ = 17.17, $\theta_5$ = 24.84	390.26	1.01	230.29

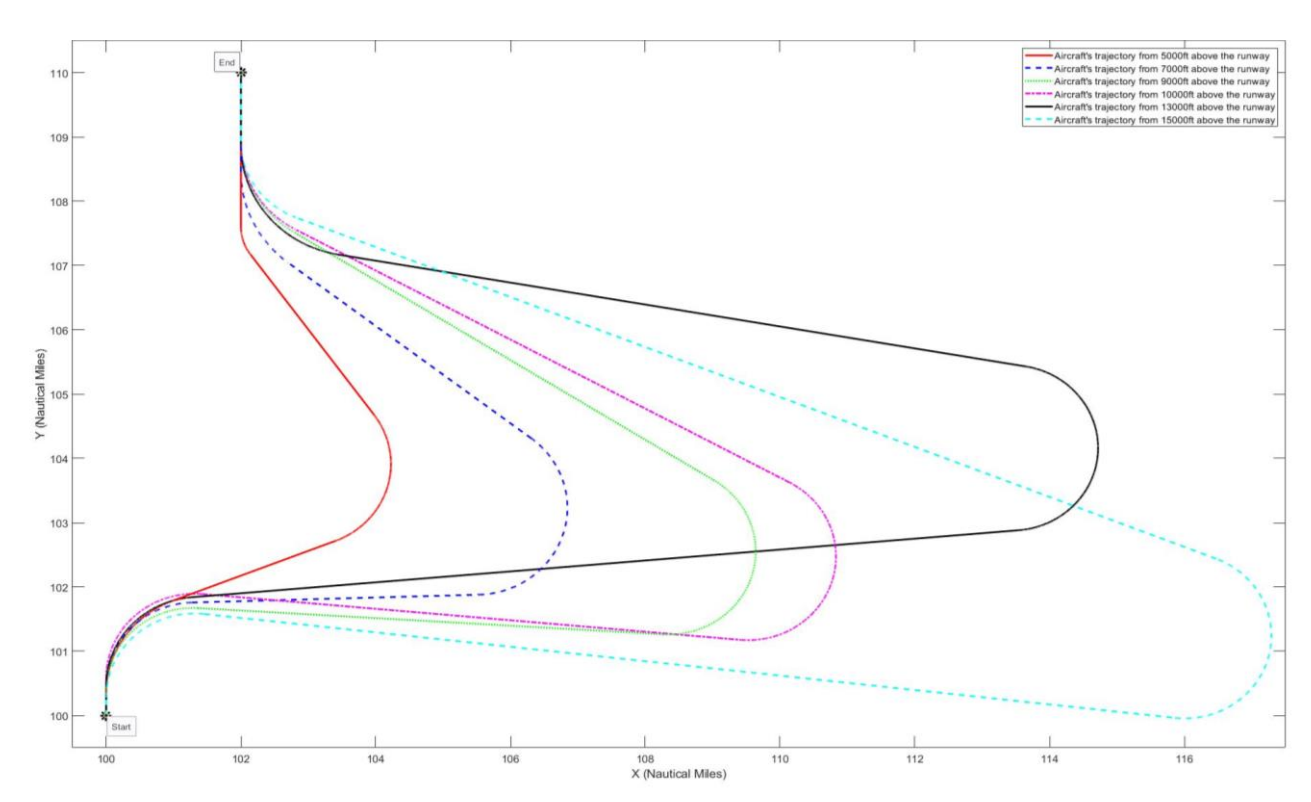


Figure 11 – Lateral profile of emergency trajectories for different initial aircraft heights (Scenario 2).

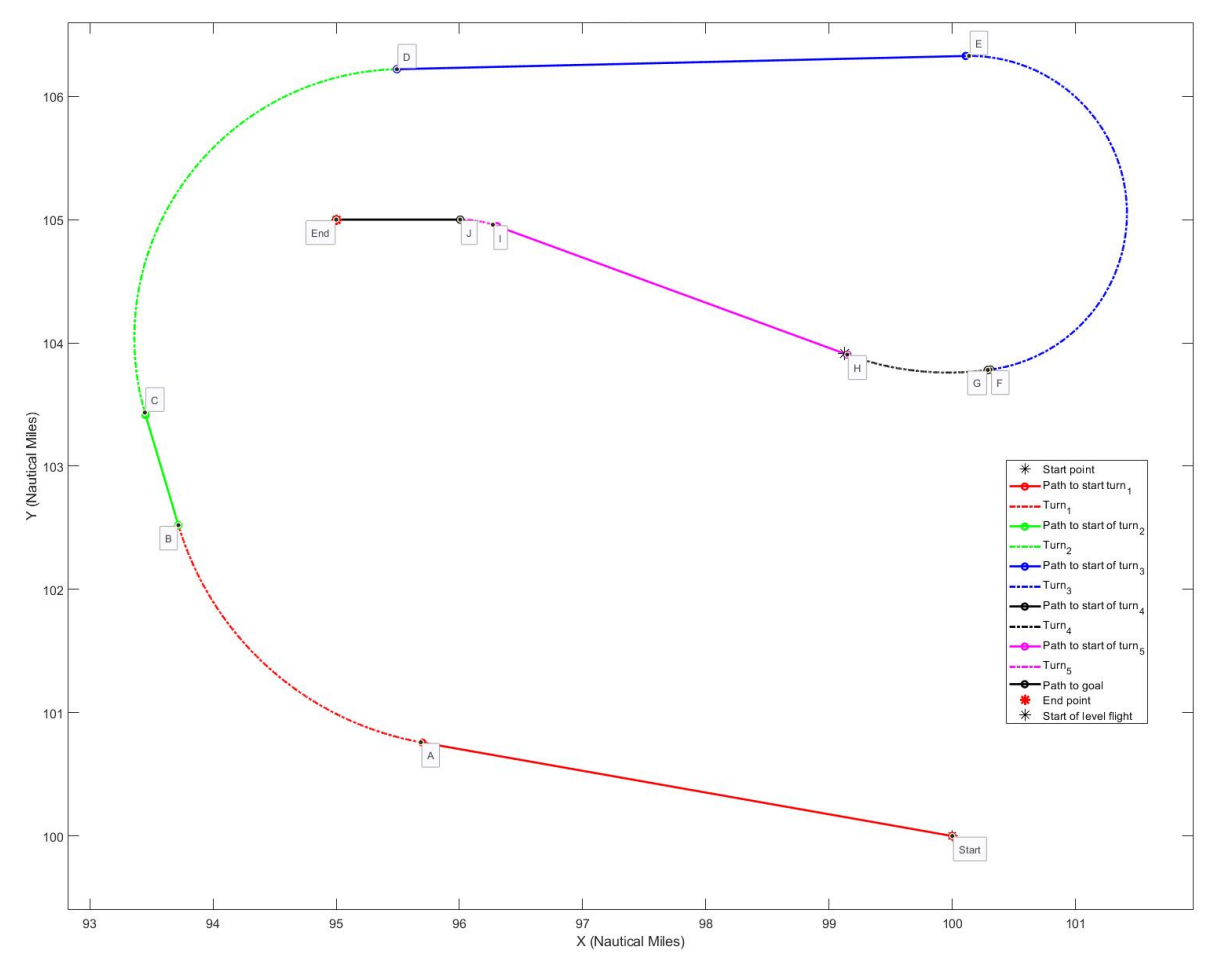


Figure 12 – Lateral profile of emergency trajectory (Scenario 9).

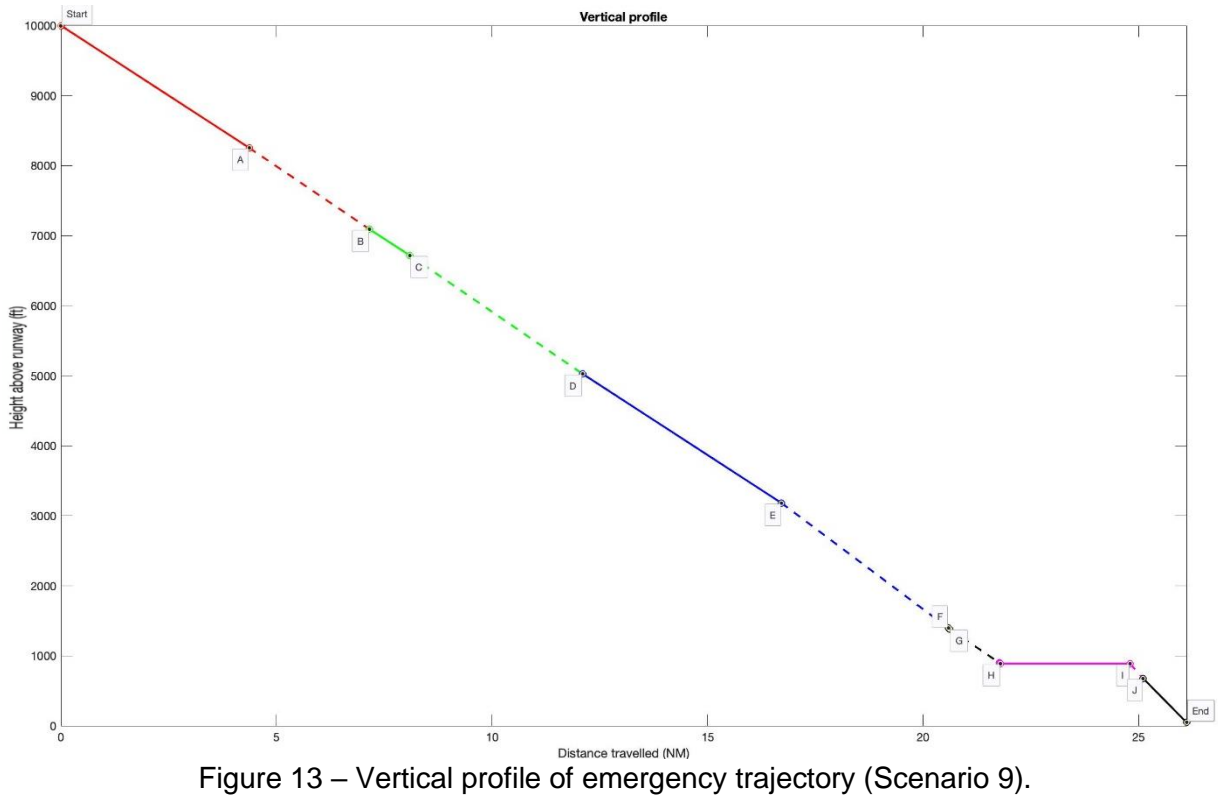


Table 6 – Results associated with the fitness function for different numbers of waypoints (Scenario 5).

Number of waypoints	$\theta_i$ (°)	Ø <sub>i</sub> (°)	∆ <i>HDG</i> (°)	d <sub>f</sub> (NM)	Execution time (s)
3	$\theta_1$ = 24.04, $\theta_2$ = 29.28, $\theta_3$ = 28.97	$\emptyset_1 = 6.96, \ \emptyset_2 = 63.12, \ \emptyset_3 = 169.92$	240.00	1.00	179.36
4	$\theta_1$ = 29.17, $\theta_2$ = 30.00, $\theta_3$ = 28.81, $\theta_4$ = 29.92	$\emptyset_1 = 7.67, \ \emptyset_2 = 120.40, \ \emptyset_3 = 42.54, \ \emptyset_4 = 160.18$	330.79	1.39	100.92
5	$\theta_1$ = 26.83, $\theta_2$ = 29.34, $\theta_3$ = 27.76, $\theta_4$ = 25.32, $\theta_5$ = 30.00	$\emptyset_1 = 0.33, \ \emptyset_2 = 59.98, \ \emptyset_3 = 97.80, \ \emptyset_4 = 108.63, \ \emptyset_5 = 138.82$	405.56	1.00	86.87

Table 7 – Results associated with the fitness function for different numbers of waypoints (Scenario 6).

Number of waypoints	θ <sub>i</sub> (°)	Ø <sub>i</sub> (°)	Δ <i>HDG</i> (°)	d <sub>f</sub> (NM)	Execution time (s)
3	$\theta_1$ = 18.52, $\theta_2$ = 19.53, $\theta_3$ = 28.84	$\emptyset_1 = 39.08, \ \emptyset_2 = 105.94, \ \emptyset_3 = 111.85$	256.87	5.39	186.41
4	$\theta_1$ = 29.98, $\theta_2$ = 28.83, $\theta_3$ = 24.45, $\theta_4$ = 12.18	$\emptyset_1 = 14.11, \ \emptyset_2 = 128.22, \ \emptyset_3 = 125.77, \ \emptyset_4 = 33.34$	301.44	2.81	90.22
5	$\theta_1$ = 26.71, $\theta_2$ = 28.24, $\theta_3$ = 23.53, $\theta_4$ = 28.95, $\theta_5$ = 19.31	$\emptyset_1 = 27.66, \ \emptyset_2 = 120.82, \ \emptyset_3 = 0.01, \ \emptyset_4 = 118.20, \ \emptyset_5 = 19.96$	286.65	1.18	90.22

Table 8 – Results associated with the fitness function for different numbers of waypoints (Scenario 17).

Number of waypoints	θ <sub>i</sub> (°)	Ø <sub>i</sub> (°)	∆ <i>HDG</i> (°)	d <sub>f</sub> (NM)	Execution time (s)
3	$\theta_1 = 7.21, \ \theta_2 = 25.06, \ \theta_3 = 13.55$	$\emptyset_1 = 14.77, \ \emptyset_2 = 73.87, \ \emptyset_3 = 133.64$	222.28	4.09	178.68
4	$\theta_1 = 20.29,  \theta_2 = 19.51, \\ \theta_3 = 4.66,  \theta_4 = 22.14$	$\emptyset_1 = 15.40, \ \emptyset_2 = 61.67, \ \emptyset_3 = 27.36, \ \emptyset_4 = 118.63$	223.06	5.59	87.08
5	$\theta_1 = 29.25, \ \theta_2 = 18.44, \ \theta_3 = 29.97, \ \theta_4 = 29.91, \ \theta_5 = 15.51$	$\emptyset_1 = 54.99, \ \emptyset_2 = 0.00, \ \emptyset_3$ = 103.35, $\emptyset_4 = 103.89,$ $\emptyset_5 = 100.54$	362.77	1.21	84.43

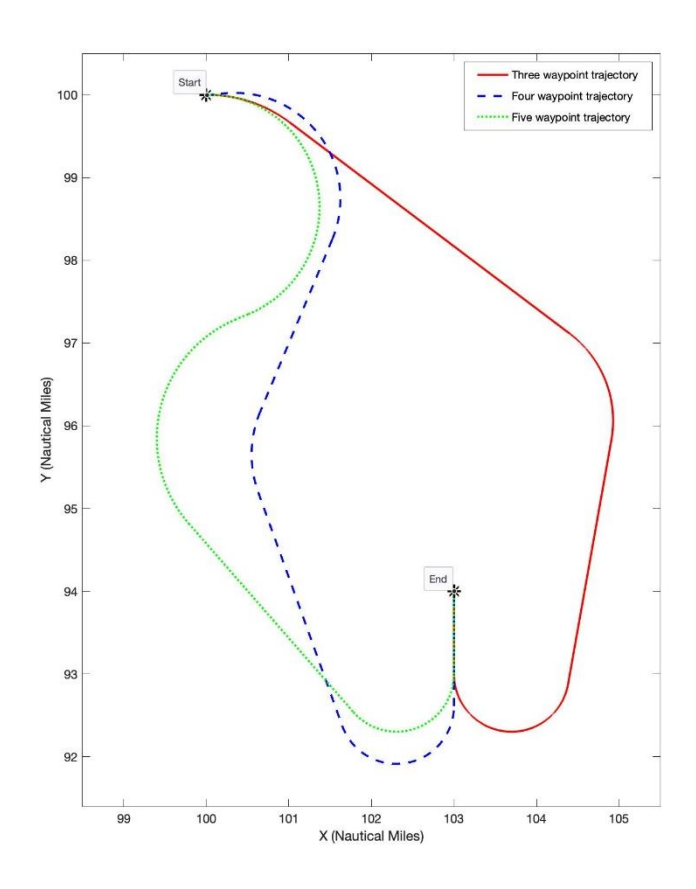


Figure 14 – Lateral profile of emergency trajectory for different numbers of waypoints (Scenario 5).

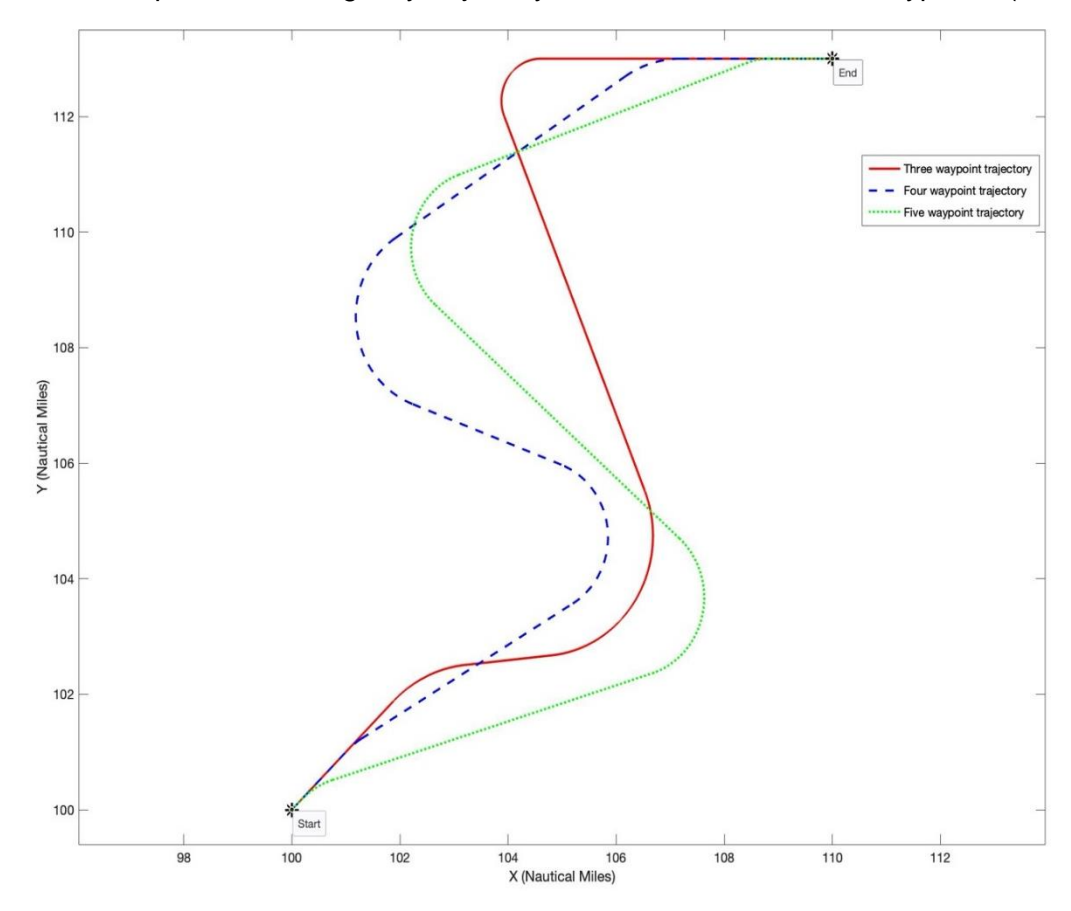


Figure 15 – Lateral profile of emergency trajectory for different numbers of waypoints (Scenario 6).

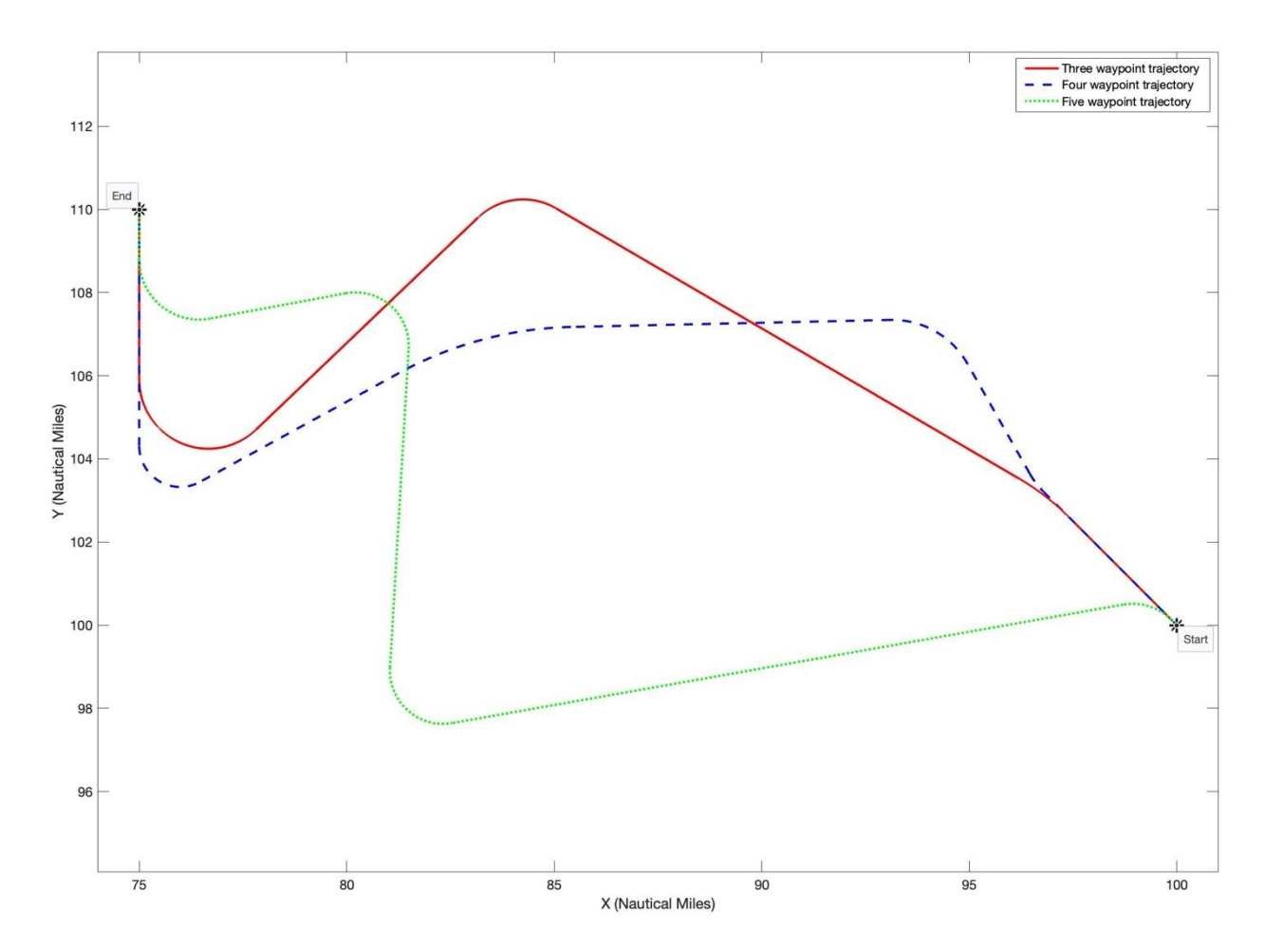


Figure 16 – Lateral profile of emergency trajectory for different numbers of waypoints (Scenario 17).

### 6. Conclusions and future work

This study adopted a GA to find a feasible glide path for large transport aircraft in the event of an emergency landing due to TLOT. The GA can be configured to generate trajectories with different numbers of waypoints and the simulation results show that it can provide solutions in various scenarios while respecting the aircraft's performance capabilities and absorbing any excess energy. The proposed trajectories can be executed by the on-board automation but are also simple enough to be flown by the flight crew if necessary. Future work will include the integration of wind in the trajectory planner, and the development of a cockpit display for pilot interaction.

#### 7. Acknowledgements

The authors of this article would like to acknowledge the project: "Setting up of transdisciplinary research and knowledge exchange (TRAKE) complex at the University of Malta (ERDF.01.124)" which is being co-financed through the European Union through the European Regional Development Fund 2014 – 2020.

# 8. Contact Author Email Address

jason.gauci@um.edu.mt

## 9. Copyright Statement

The authors confirm that they, and/or their company or organization, hold copyright on all of the original material included in this paper. The authors also confirm that they have obtained permission, from the copyright holder of any third party material included in this paper, to publish it as part of their paper. The authors confirm that

they give permission, or have obtained permission from the copyright holder of this paper, for the publication and distribution of this paper as part of the ICAS proceedings or as individual off-prints from the proceedings.

#### References

- [1] Rahman A., Zammit B. & Gauci J., "A Fuzzy-based Site Selection Framework for Emergency Landings of Commercial Aircraft", AIAA Aviation Forum, Chicago, Illinois & Online, 27 June-1 July, 2022.
- [2] Atkins E. M., Portillo I. A. & Strube M. J., "Emergency Flight Planning Applied to Total Loss of Thrust", Journal of Aircraft, vol. 43, no. 4, pp. 1205-1216, 2006. Accessed: Dec. 28, 2023. doi: 10.2514/1.18816. [Online]. Available: https://doi.org/10.2514/1.18816.
- [3] Atkins E. M., "Emergency Landing Automation Aids: An Evaluation Inspired by US Airways Flight 1549", in *AIAA Infotech* @*Aerospace 2010*, 2010, [Online]. Available: https://arc.aiaa.org/doi/abs/10.2514/6.2010-3381.
- [4] Saswata P., Hole F., Zytek A. & Varela C. A., "Flight Trajectory Planning for Fixed-Wing Aircraft in Loss of Thrust Emergencies", in *Second International Conference on InfoSymbiotics / DDDAS (Dynamic Data Driven Applications Systems)*, 2017, [Online]. Available: https://arxiv.org/abs/1711.00716.
- [5] Saswata P., Hole F., Zytek A. & Varela C. A., "Wind-Aware Trajectory Planning for Fixed-Wing Aircraft in Loss of Thrust Emergencies," in 2018 IEEE/AIAA 37th Digital Avionics Systems Conference (DASC), London, UK, 2018, pp. 1-10, doi: 10.1109/DASC.2018.8569842.
- [6] Fallast A. & Messnarz B., "Automated trajectory generation and airport selection for an emergency landing procedure of a CS23 aircraft", CEAS Aeronaut J 8, pp. 481–492, 2017, [Online]. Available: https://doi.org/10.1007/s13272-017-0252-5.
- [7] Hongying Wu, Nayibe Chio Cho, H. Bouadi, Lunlong Zhong & F. Mora-Camino, "Dynamic programming for trajectory optimization of engine-out transportation aircraft," 2012 24th Chinese Control and Decision Conference (CCDC), Taiyuan, 2012, pp. 98-103, [Online]. Available: doi: 10.1109/CCDC.2012.6244015.
- [8] Snoeij, V., "Emergency trajectory management for transport aircraft", M.S. thesis, Faculty of Aerospace Engineering, TU Delft, 2016, [Online]. Available: http://resolver.tudelft.nl/uuid:b68ac652-edcc-43ac-8bc0-bbba4113e047.
- [9] Meng S., Xiang J., Luo Z. et al., "A novel trajectory planning strategy for aircraft emergency landing using Gauss pseudospectral method", Control Theory Technol. 12, pp. 393–401, 2014. [Online]. Available: https://doi.org/10.1007/s11768-014-3162-7.
- [10] Miwa M., Tsuchiya T., Yonezawa S., Yokoyama N. & Suzuki S., "Real-Time Flight Trajectory Generation Applicable to Emergency Landing Approach", Transactions of the Japan Society for aeronautical and space sciences, vol. 52, no. 175, pp. 21-28, 2009. doi: 10.2322/tjsass.52.21.
- [11] Avrenli K. A. & Dempsey B. J., "A kinematic approach to segmented-trajectory generation for the total loss of thrust emergency", Aviation, vol. 19, no. 3, pp. 138-149, 2015. [Online]. Available: https://doi.org/10.3846/16487788.2015.1104847.
- [12] Adler A., Bar-Gill A. & Shimkin N., "Optimal flight paths for engine-out emergency landing," in 2012 24th Chinese Control and Decision Conference (CCDC), Taiyuan, China, 2012, pp. 2908-2915, doi: 10.1109/CCDC.2012.6244461.
- [13] Airbus Quick Reference Handbook, Airbus S.A.S., France, 2019.
- [14] MathWorks R2024a Documentation Page, [Online]. Available: https://www.mathworks.com/help/gads/ga.html